2-Dimensional Metal Zn Nanostructure Electrodes for High-Performance Zn Ion Supercapacitors

Geon-Hyoung An[a,b,1], John Hong[c,1], Sangyeon Pak[d], Yuljae Cho[e], Sanghyo Lee[e], Bo Hou[e] and SeungNam Cha[d,*]

[a]Department of Energy Engineering, Gyeongnam National University of Science and Technology, Jinju, Republic of Korea

[b]Future Convergence Technology Research Institute, Gyeongnam National University of Science and Technology, Jinju, Republic of Korea

[c]Department of Engineering Science, University of Oxford, Parks Road, Oxford OX1 3PJ, United Kingdom

[d]Department of Physics, Sungkyunkwan University, Suwon, Gyeonggi-do, 16419, Republic of Korea

[e]Electrical Engineering Division, Department of Engineering, University of Cambridge, 9 JJ Thomson Avenue, Cambridge, CB3 0FA, United Kingdom

Keywords: two-dimensional structures, hierarchical structures, flexible devices, supercapacitors

[*]Corresponding author.

E-mail address: chasn@skku.edu

[1]These authors contributed equally to this work.

Abstract

Recent supercapacitors show a high power density with long-term cycle life time as energy-powering applications. Supercapacitor based on a single metal electrode accompanying multivalent cations, multiple charging/discharging kinetics, and high electrical conductivity can be promising energy-storing system with replacing conventionally used oxide and sulfide materials. Here, we report a hierarchically nanostructured two-dimensional (2D)-Zn metal electrode-ion supercapacitor (ZIC) which significantly enhances the ion diffusion ability and overall energy storage performance. Those nanostructures can also be successfully plated on various flat-type and fiber-type current collectors by a controlled electroplating method. The ZIC exhibits excellent pseudo-capacitive performance with a high energy density of 208 Wh kg^{-1} and a power density from 500 W kg^{-1}, which are greatly higher than those of previously reported supercapacitors with oxide and sulfide materials. Furthermore, the fiber-type ZIC also shows high energy-storing performance, outstanding mechanical flexibility and good waterproof ability without any significant capacitance degradation during bending tests. These results highlight the promising possibility of nanostructured 2D Zn metal electrodes with the controlled electroplating method for future energy storage applications.

1. Introduction

Since its introduction in the very first electrochemical energy storage, supercapacitors with oxide and sulfide electrode materials have been regarded as promising candidates for energy delivering system.[1-3] Alternatively, instead of using oxide and sulfides electrode materials, pure metal materials can lead to the better performance in electrochemical energy storage than the previous electrode materials due to their multivalent cations and high electrical conductivity.[4-8] In principal, pure metal supercapacitors can induce multiple charging/discharging electrons based on their oxidation state of metal cations, which can attribute to a high energy density.[6-8] Metal electrodes can also utilize highly reversible redox-reactions (the metal deposition and dissolution reactions between metal cations and metal electrode), resulting in excellent cycling stability. Finally, the high conductivity of metal electrode also can increase the overall energy storing performance.

Among various metal electrode candidates, Zinc (Zn) metal electrode-ion supercapacitors (ZICs) with Zn^{2+} electrolyte ion have become of the great interest owing to their attractive features such as the high electrical conductivity of Zn, good reversible reactions from the deposition and the stripping of Zn^{2+}, low redox potential of −0.76 V (versus standard hydrogen electrode), long-operation lifetime as well as the safe, cheap and eco-friendly properties of Zn materials.[9-16] As the first proof of concept, Wang et.al.[9] reported that the simple Zn foil supercapacitor can show outstanding electrochemical energy storing properties, including the high energy density and stability. However, the Zn foil ZICs show the poor rate retention (the low power density) compared to those of other reported supercapacitors due to the low diffusion ability of Zn ions along with the simple planar structure of the Zn metal foil.[9-12] However, to date, there have been no viable and practical studies showing notable ion diffusion property and overall energy storage performance with ZIC.

In this paper, we firstly propose two-dimensionally and hierarchically nanostructured Zn (2D-Zn) metal electrode of ZICs. The 2D-Zn metal electrodes were carefully obtained by a voltage-tailored

electroplating method to optimize their 2D morphology and hierarchical structure density on a micron porous current collector. First, those unique 2D Zn nanostructures can provide shorter diffusion paths of Zn ions, which results in a high-power density (500 to 20,000 W kg^{-1}). Additionally, an enlarged surface area and metal-like conductivity of 2D-Zn can exhibit an excellent energy density (208 Wh kg^{-1}) and long cycle-life with a remarkable cycling stability (~99%). Especially, due to the low standard electrode potential (–0.76 V) of Zn, 2D-Zn metal can be easily deposited on any form factor even on a fiber-type current collector which can be used for next generation energy storage applications. The fiber-type 2D-Zn metal electrodes prepared on flexible carbon cloths show the exceptional flexibility and knittability against external and environmental conditions, indicating that this unique deposition method and the resulting hierarchical 2D-Zn nanostructures can be promising for superior and practical supercapacitors.

2. Results and Discussions

As shown in Figure 1a, a full cell 2D-Zn//AC (AC, activated carbon) asymmetric supercapacitor can store charges by both the surface Faradaic redox reactions between Zn/Zn^{2+} on the anode and the formation of electric double-layers with electrolyte ions (Zn ions and sulfate ions) on the cathode (Activated carbon, AC). For the flat-type ZICs, a Ni foam was used for the current collector due to its microstructure, good chemical/mechanical stability and high electrical conductivity.[17-21] As illustrated in Figure 1b, the novel 2D-Zn electrodes were successfully prepared by the voltage-tailored electroplating method on the Ni foam.

Compared to the other reported synthetic methods, electroplating is well known as a very simple and facile synthetic method for depositing single phase metallic materials and other material composites by controlling the concentration and precursor of solutions. Moreover, it can be applied to any metallic substrate even on flat, curved, and rough substrates.[22-25] Especially, in this work, the driving forces of Zn deposition on a Ni metal substrate have been studied. It is usually difficult to induce hierarchically

interconnected metal nanostructures and optimized morphology design with controlled synthetic parameters for material nucleation and crystal growth, which provide the favorable electrochemical energy storing performance. Therefore, to obtain the hierarchically interconnected nanostructured 2D-Zn, an optimized initial voltage and step-wise additional voltage were carefully applied. The diverse level of nucleation growths can be well controlled by the precise initial operation voltage and additional voltage can alter the driving force for the subsequent level of crystal growths. With the too low operation voltage, the low level of metal nucleation sites will be induced on substrates and limit the following crystal growth. However, as the operation voltage is too high, the excess amount of metal nucleation sites will be deposited on substrates, and the relatively large and bulk morphology of metal would be obtained. To optimize the operation voltages, we compare the two different operation voltages (1.0 V (2D-Zn/1.0) and 1.8 V (2D-Zn/1.8)) as the initial deposition conditions. Figure 2a-b show the deposition current curves of 2D-Zn/1.0 and 2D-Zn/1.8 during the electroplating method. The electroplating procedure takes place upon the mitigating Zn^{2+} ions towards the target substrate and exceed the activation energy of Zn deposition when the system is driven out of electrostatic equilibrium owing to the electric field generated in the electrolyte solution. At the operation voltage of 1.0 V, the current curve was increased during 20 sec and subsequently reached to its equilibrium level, which is not high enough to induce spontaneous Zn mitigation and nuclei formation, leading to the not-well coated Zn electrode (even not structured Zn). It proves that their might need a high overpotential to grow to the critical size of Zn nuclei which is demanded for a new phase at initial electrostatic plating process.[26-28] Meanwhile, at the operation voltage of 1.8 V, the initial current is decreased due to the introduction of electrostatic double-layer (at the interface between electrode and electrolyte) as well as the formation of Zn nuclei.[26-28] This phenomenon of deposition current represents that the uniform plating process has been initiated. Subsequently, the current reaches to the equilibrium and is well retained, implying that the formation of Zn nuclei leads to the disbandment of initial double-layer. Also, scanning electron microscopy (SEM) was used to investigate the deposited nanostructures of 2D-Zn/1.0 (Figure 2d) and 2D-Zn/1.8 (Figure 2e), respectively. Figure 2d shows that the 2D-Zn/1.0 electrode does not have the uniform 2D structures. On the contrary,

at the operation voltage of 1.8 V, the current curve started at the highest point and saturated after 30 sec. The thick and bulk structures of 2D-Zn/1.8 was observed (Figure 2e). Therefore, we used the both operation voltage of 1.8 V for the initial nucleation growth within the short reaction time (30 sec), and 1.0 V for the crystal growth of Zn within long reaction time (300 sec) (as referred 2D-Zn/1.8/1.0). As presented in Figure 2c, the Zn seeds were uniformly decorated on surface of the Ni foam at 1.8 V for 30 sec (Figure S1) and then the operation voltage of 1.0 V was kept continued almost 300 sec to induce the oriented crystal growth of Zn. The SEM image of 2D-Zn/1.8/1.0 (Figure 2f) presents the hierarchically interconnected 2D Zn nanostructures with a thin thickness of 10 ~ 25 nm and a length of 6~ 11 μm. The formation mechanism of hierarchically interconnected 2D-Zn structures may proceed along the following reasons. By controlling the step-wise deposition voltages, we can efficiently tailor the nucleation and growth of Zn on the target substrate. After applying the high voltage during short time frame (the nucleation stage), the relatively many Zn seeds can be electrically deposited on the substrate compared to the low voltage. Subsequently, lowering the plating voltage after the nucleation (growth stage) will can modify the formation rate of Zn on the deposited Zn seeds, resulting in the uniform and hierarchically structured 2D-Zn. Therefore, the step-wise electroplating methods can systematically change the structure, uniformity and density of the 2D-Zn structures on the substrate by adjusting the atomic assembly behavior. Thus, the hierarchically interconnected 2D-Zn electrodes can be fabricated through the instantaneous fast nucleation and subsequent slow growth formation of Zn.[29-31] Finally, on the surface of 2D-Zn, the networks structures are formed, being randomly distributed over the surface. As shown in Figure S2a, the schematic illustration depicts the detailed nucleation and growth stages on a target substrate during the step-wise plating process. Figure S2b-f shows the SEM images at nucleation and growth stages during the plating. Those SEM images confirm that the different seed sites and nanostructured Zn electrodes can be well-tailored by the low to high operating voltage. In addition, the electrode of 2D-Zn/1.8/1.0 was further investigated by high-resolution transmission electron microscope (HR-TEM) microscopy, as shown in Figure S3a and b. We can easily observe that the distance of parallel lattice fringes is 0.23 nm, corresponding to the (010) plane of pure Zn crystals with hexagonal

structure.[32,33] Also, the crystalline nature of 2D-Zn/1.8/1.0 was demonstrated by selected area electron diffraction (SAED) pattern (Figure S3c). The six-fold symmetrical diffraction spots correspond to the [100] zone axis, indicating that 2D-Zn/1.8/1.0 Zn nanosheets show the hexagonal crystals of pure Zn metal.[34,35]

In addition, to examine the crystal structure of 2D-Zn electrodes, X-ray diffraction (XRD) were carried out. Figure 2g shows the XRD patterns of 2D-Zn/1.0, 2D-Zn/1.8 and 2D-Zn/1.8/1.0. The two sharp diffraction peaks are observed at 44.5º, and 51.8º, corresponding to the (111) and (200) planes of face-centred metallic Ni. The diffraction peaks of 2D-ZN/1.8/1.0 at 36.2°, 38.9°, and 43.2° can be well matched with the (002), (100), and (101) planes of hexagonal Zn phase. The (002), (100), (101) index are the most intense plane of Zn and it clearly prove that the 2D-Zn has been formed along the c-axis. Its orientated growth of Zn leads to the formation of interconnected 2D nanostructure.[29-31] However, for 2D-Zn/1.0, the diffraction peaks of hexagonal Zn phase are not observed due to the small amount of Zn, indicating that the electroplating voltage of 1.0 V is not active enough to deposit the large amount of Zn. X-ray photoelectron spectroscopy (XPS) were performed to analyses the chemical states of the 2D-Zn electrodes. The XPS results of all electrodes show that the metallic Zn phase was successfully deposited (Figure 2h).[10,36] Due to no additional heat treatment, we clearly demonstrate that, by the XRD and XPS analysis, there are no multiphase zinc composites (ZnO or $Zn(OH)_2$) on the 2D-Zn electrodes, confirming that our method is highly favorable to deposit pure Zn metal without any side formation reactions on target substrates. The electrical conductivity of 2D-Zn can be close to the pure metal, guaranteeing the better electrochemical performance. The low level of oxidation states of Ni^{2+} are detected at 2D-Zn/1.0, and this is because the Zn nanostructures are not fully covered on the Ni current collector (Figure 2i).

In order to confirm the quantitative contents of 2D-Zn/1.0, 2D-Zn/1.8, and 2D-Zn/1.8/1.0, the inductively coupled plasma-mass spectroscopy (ICP-MS) analysis was carried out. The Zn/Ni atomic ratios of the as-prepared electrodes were summarized in Table S1. 2D-Zn/1.0 includes comparatively the low Zn contents, implying the insufficient deposited Zn on the Nickel substrate. On the other hand,

2D-Zn/1.8 and 2D-Zn/1.8/1.0 showed the atomic content of 30% and 26%, respectively. Within the high voltage initial potential, the structured metallic Zn was successfully deposited.

Through the novel nanostructures of Zn electrodes, we fabricated flat-type 2D-Zn//AC ZIC asymmetric supercapacitors. For the full cell fabrication, active carbon (AC) was used as the cathode material. The as-prepared ACs shows the amorphous morphology and has the large surface area of 2,201 $m^2\ g^{-1}$ (Figure S4a). Also Figure S4b shows the XRD data of the ACs. Figure 3a shows Nyquist plots by electrochemical impedance spectroscopy (EIS) analysis. It can confirm that the charge transfer resistance (R_{ct}) of 2D-Zn/1.8 and 2D-Zn/1.8/1.0 in a high-frequency region (a diameter of semi-circle) is low than that of 2D-Zn/1.0, indicating that hierarchically interconnected Zn structures improve the electrical contact and charge transfer capability.[17-19] Furthermore, in a low-frequency region, the straight slop of the plot curves implies the ionic diffusion behavior at the surface between electrode and electrolyte (called Warburg impedance),[17-19] The steepest slope of 2D-Zn/1.8/1.0 demonstrates that the electrode has the lowest Warburg impedance and guarantees the best ion diffusion kinetics through the electrode. Figure 3b shows a cyclic voltammetry (CV) curve with a voltage range of 0.2 to 1.8 V. The redox humps on the CV curves of 2D-Zn/1.8 and 2D-Zn/1.8/1.0 electrodes indicate the Faradaic redox reactions from the deposition/stripping of Zn ions ($Zn \leftrightarrow Zn^{2+} + 2e^-$).[9-13] As shown in Figure S5, the CV curves of 2D-Zn/1.8 and 2D-Zn/1.8/1.0 electrodes with an increased scan rates retained their original profiles, signifying the Zn ion redox reaction. Moreover, Figure S6 shows the galvanic charge discharge curves of the as-prepared Zn electrodes. The GCD curves have the almost similar charging and discharging times, indicating their outstanding coulombic efficiency performance. In contrast, the CV curve of 2D-Zn/1.0 shows no significant redox humps. This result might imply that the relatively low amount of Zn and low surface area from the not structured Zn on the substrate is insufficient to drive noticeable electrochemical reactions. Also, the small amount of Zn cannot maintain the cell charge balance within the full cell configuration with the AC-based cathode, leading to no significant redox humps. For the direct comparison of the morphology and electrochemical performance of 2D-Zn, five

electrodes with different morphology (a thin Zn foil (no structures), 2D-Zn/1.0 (no Zn on a substrate), 2D-Zn/1.8/30sec (basic backbone structures), 2D-Zn/1.8/1.0 (hierarchical structures) and 2D-Zn/1.8/360sec (bulky structures) were electrochemically tested through a two-electrode cell system. As shown in Figure 3c, the specific capacitance of the electrodes was calculated by the GCD curves and a mass of the active materials. In terms of capacitance performance, the 2D-Zn/1.8/1.0 electrode can reach to the highest specific capacitance of 468 F g^{-1} at a current density of 0.5 A g^{-1}. In addition, the specific capacitance of 2D-Zn/1.8/1.0 at a high current density of 20.0 A g^{-1} can maintain to 150 F g^{-1}. In contrast, the 2D-Zn/1.0 electrode does not include a large amount of Zn plating on the Ni substrate without the specific structures. Consequently, it has the negligible electrochemical reactivity with Zn ions. The specific capacitance of the 2D-Zn/1.8/30sec and 2D-Zn/1.8 electrode are 436 F g^{-1} and 406 F g^{-1} at a current density of 0.5 A g^{-1}, respectively, which are lower than that of the 2D-Zn/1.8/1.0 electrode (Figure S7). These results indicate that the additional 2nd electroplating step with an operating voltage of 1.0 V results in much larger surface area after the initial electroplating under an operating voltage of 1.8 V. The 2D-Zn/1.8 electrode represents the lower capacitance than the 2D-Zn/1.8/30s electrode. This is because the 2D-Zn/1.8 has the much thicker and bulky 2D structures which might decrease the overall active sites on the surface of electrodes. According to the results of rate retention, the calculated rate retention value of the 2D-Zn/1.8/1.0 with the hierarchical structure has the largest value (~32 %) and is much larger than the values for the 2D-Zn/1.8/30sec (~13.7%) and the 2D-Zn/1.8 (~12.2%), which is mainly due to the microstructures of the 2-D Zn electrodes. This implies that the hierarchical structure of 2D-Zn/1.8/1.0 provides a sufficient electrolyte ion contact and can thus enhance the kinetics of ion diffusion. Consequently, the induced 2D-nanostructures can improve the electrochemical capacitance and the charge-transfer kinetics. Thus, to build the hierarchically interconnected Zn structures, the two-step process of electroplating is highly favorable to increase the overall energy-storing performance. As shown in Figure S8, the flat and thin Zn foil shows the lowest capacitance (280 F g^{-1} at a current density of 0.5 A g^{-1}), rate retention (~ 1% from a current density from 0.5 A g^{-1} to 150 F g^{-1}), and the flattest EIS Warburg impedance, demonstrating the importance of structuring of electrodes. As highlighted in a

Ragone plot (Figure 3d), The electrode of 2D-Zn/1.8/1.0 shows a maximum energy density of 208 W h kg^{-1} at a power density of 500 W kg^{-1}, and the maximum of 20,000 W kg^{-1} can be acquired with a remaining energy density of 66 W h kg^{-1}, which are much higher than those of the previously reported supercapacitors.[37-46] Furthermore, the cycling stability of 2D-Zn/1.8/1.0 was tested at a current density of 10.0 A g^{-1} over 10,000 cycles (Figure 3e). The 2D-Zn/1.8/1.0 electrode shows the excellent cycling stability with a capacitance retention of 99% even after 10,000 cycles.[37,38,40-48] Additionally, as shown in Figure S9, the charge transfer resistance and Warburg impedance by the EIS measurement are unaltered even after 5,000 and 10,000 cycling tests, demonstrating the excellent electrochemical kinetics and stability of 2D-Zn ZICs. In previous studies including Zn foil-based ZICs, a zinc sulfate hydroxide hydrate as $Zn_4SO_4(OH)_6 \cdot 5H_2O$ was formed on the surface of electrodes when the pH of the electrolyte solutions increases to ~5.3 and then the precipitation will redissolve when the pH decreases during the cycling process.[11] However, in our electrochemical systems, we did not observe precipitation/dissolution reactions of a zinc sulfate hydroxide hydrate on the surface of electrodes. The 2D-Zn electrodes were cycled along with the different cut-off voltage, and the XRD experiments of each electrode were carried out (Figure S10), indicating that there is no formation of zinc sulfate hydroxide hydrates. We can assume that the non-active Ni current collectors with Zn ions might be act as the stable backbone and electron paths, leading to the stable electrochemical process without side reactions. Importantly, as this deposition method can be easily compatible with various conductive substrates for energy storage applications, this process can also be applied on other flexible conductive substrates with a variety of platforms, successfully fabricating the hierarchically interconnected 2D Zn nanostructures.

Therefore, the voltage tailored electroplating method can be systemically applied for the successful formation of the 2D-Zn metal on the flexible fiber substrate. The fiber-type 2D-Zn ZICs also show the excellent energy storing performance due to the well-ordered 2D nanostructures. As illustrated in Figure 4a and Figure S11, the 2D-Zn structures on carbon fibers (2D-Zn@CF) were successfully fabricated as the anode. AC on carbon fibers (AC@CF) were also conducted by a solution casting method as the

cathode. To fabricate the full cell fiber-type ZICs, the AC@CF electrode was enclosed by cellulose papers as the separator (Figure S12) and subsequently, the AC@CF electrode was additionally weaved by the 2D-Zn@CF anode. The gel electrolyte (Figure S13) was prepared by the homogeneous mixture of 1M zinc sulfate ($ZnSO_4$) and poly(vinyl alcohol) (PVA) in deionized water. The $ZnSO_4$/PVA gel electrolyte was carefully coated on the Zn//AC cells. Finally, thermally shrinkable tubes were covered to encapsulate the fiber-type ZICs for chemical and physical protection. The areal length of the fiber-type ZICs is about 15 cm. The individual CF has a flat surface and a diameter of 8 ~ 9 ㎛ (Figure S14). The poor surface wettability of CFs can hinder the homogeneous nucleation and growth of electroplated metal materials (Figure S15). Therefore, the surface functionalization of the CFs was carried out to modulate the surface energy and wettability by a surface chemical oxidation method. After the surface functionalization, the percentage of oxygen-containing functional groups on the CFs is increased from 21.7 % to 40.7 %, implying the favorable surface status of the CFs (Figure S16). Figure 4b represents SEM images of the 2D-Zn@CF cells under the different electroplating voltage conditions. At an operation voltage of 1.0 V, the interconnected nanostructures of Zn were successfully plated with a thin thickness of 10 ~ 25 nm and a length of 1 ~ 3 ㎛. In contrast, at a voltage of 0.7 V, the plating potential is not enough to form hierarchical nanostructures and leads to the flat coverage of Zn (Figure S17a and b). On the other hand, at a voltage of 1.5 V, the expected two-dimensional Zn nanostructures are not observed except the bulk morphology of Zn (Figure S17c and d). As shown in Figure 4c, the XRD peaks of 2D-Zn@CF are well indexed to the crystal structure of hexagonal Zn. Also, the chemical state of metallic Zn from the 2D-Zn@CF samples is proved by XPS analysis (Figure 4d). To investigate the contents of Zn on the CFs, thermogravimetric analysis was also carried out (Figure S18). The 2D-Zn@C exhibits the weight loss of 52 %, signifying the presence of Zn atoms. The electrochemical behaviors of fiber-type 2D-Zn ZIC were investigated by CV curves and GCD curves (Figure S19), which are in good agreement with the flat-type ZIC results. The fiber-type 2D-Zn ZIC can achieve to a higher specific capacitance of 56 to 24 mF cm^{-2}

at a current density of 0.05 to 3.0 mA cm^{-2} (Figure S20). Moreover, the EIS results also clearly confirm that the interconnected nanostructures of 2D-Zn provide the favorable ion diffusion ability (Figure S21).

The energy and power density were calculated as highlighted in a Ragone plot (Figure 5a). The fiber-type ZIC have a high energy density of 25 to 12 μWh cm^{-2} and also presents a good power density ranging from 50 to 3,000 μW cm^{-2} [49-61] as well as high cycling stability over 10,000 cycles, which are superior than the other reported fiber-type supercapacitors (Figure 5b).[50-52,54-57,60] After cycling tests, the structural decomposition of both ZIC 2D-Zn/1.8/1.0 and 2D-Zn@CF was investigated using SEM (Figure S22). The original morphology 2D-Zn was well maintained even after 10,000 cycles, indicating that the corresponding dendrites might not be formed on the surface of Zn. Therefore, the Zn ion energy storing applications are the best candidate for the stable and long-term operation. Figure 5c also represents that the fiber-type ZIC can maintain the original energy storing performance even when it is folded and knotted, which demonstrates a high mechanical flexibility of fiber-type ZIC. These results confirm that the voltage-tailored electroplating method is a powerful engineering tool for fabricating flexible energy storage applications. Moreover, the waterproof capability of the ZICs was also examined. The electrochemical performance of the fiber-type ZICs was evaluated under water immersion, as shown in Figure 5d. The capacitance of the ZICs is well maintained under water for a long-time scale use. The two fiber-type ZICs were connected in series or parallel (Figure S23a and b). The charge/discharge voltage range is doubled when two devices are in series, and the overall GCD time increased by two times when they are in parallel. The multiple fiber-type ZICs (up to 5 devices) were connected in parallel (Figure S23c), and the overall capacitance was proportionally increased according to the number of the connected ZIC devices. Finally, we demonstrated that the multiple fiber-type ZICs can successfully power up a red-light emitting diode (LED) even though they are strongly knotted under water (Figure 5e).

3. Conclusions

In summary, we reported hierarchically interconnected 2D Zn nanostructures by an electroplating method to improve the overall ionic and electronic transport performance of supercapacitors. The flat-type ZIC achieves a high energy density of 208 Wh kg^{-1} in a high-power density from 500 W kg^{-1} as well as an excellent long-term cyclability over 10,000 cycles. In addition, the fiber -type ZIC shows the unprecedented energy storage performance with a high energy density of 25 μWh cm^{-2} at a high-power density of 50 μW cm^{-2}, outstanding cycling stability, excellent mechanical flexibility and good waterproof properties. We attribute the outstanding performance to (i) the nano-architecture that provide electrochemically large active sites, leading to the high energy storing performance and (ii) the enhanced ionic transport from the hierarchically interconnected 2D-Zn nanostructures. Hence, this study demonstrates that the voltage-tailored electroplating method and the following 2D-Zn structures can provide new insights into future wearable energy storage applications and might be applied to other devices such as zinc-ion anode batteries.

Acknowledgments

This work was supported by the National Research Foundation of Korea(NRF) grant funded by the Korea government(MEST) (No. 2019R1A2C1005930). This research was also supported by the European Research Council under the European Union's Seventh Framework Programme (FP/2007- 2013)/Grant Agreement no. 685758, Project ‘1D-NEON’.

References

[1] P. Simon, Y. Gogotsi and B. Dunn, *Science* **2014**, 343, 1210.

[2] G. Wang, L. Zhang and J. Zhang, *Chem. Soc. Rev.* **2012**, 41, 797.

[3] P. Simon and Y. Gogotsi, *Nat. Mater.* **2008**, 7, 845.

[4] M.-S. Balogun, W. Qiu, W. Wang, P. Fang, X. Lu and Y. Tong, *J. Mater. Chem. A* **2015**, 3, 1364.

[5] M. Yu, Z. Wang, Y. Han, Y. Tong, X. Lu and S. Yang, *J. Mater. Chem. A* **2016**,4, 4634.

[6] K. Li, Y. Shao, S. Liu, Q. Zhang, H. Wang, Y. Li, R.B. Kaner *Small* **2017**, 13, 1700380.

[7] X. Cao, L. Wang, J. Chen and J. Zheng, *ChemElectroChem* **2018**, 5, 1.

[8] V. Aravindan, M. Ulaganathan and S. Madhavi, J. *Mater. Chem. A* **2016**, 4, 7538.

[9] H. Wang, M. Wang and Y. Tang, *Energy Storage Materials* **2018**, 13, 1.

[10] G.-H. An, S.N. Cha, J. I. Sohn, *Appl. Surf. Sci.* **2019**, 467–468, 1157.

[11] L. Dong, X. Ma, Y. Li, L. Zhao, W. Liu, J. Cheng, C. Xu, B. Li, Q.-H. Yang, F. Kang, *Energy Storage Materials* **2018**, 13, 96.

[12] Y. Tian, R. Amal and D.-W. Wang, *Frontiers in Energy Research* **2016**, 4, 1.

[13] S. Chen, L. Ma, K. Zhang, M. Kamruzzaman, C. Zhi, J.A. Zapien, *J. Mater. Chem. A* **2019**, 7, 7784.

[14] G. Sun, H. Yang, G. Zhang, J. Gao, X. Jin, Y. Zhao, L. Jiang and L. Qu, *Energy Environ. Sci.* **2018**, 11, 3367

[15] J. Wang, F. Li, F. Zhu, O.G. Schmidt, *Small Methods* **2018**, 14, 1800367.

[16] P. Zhang, Y. Li, G. Wang, F. Wang, S. Yang, F. Zhu, X. Zhuang, O.G. Schmidt, X. Feng, *Adv. Mater.* **2018**, 18, 1806005.

[17] G.-H. An, D.-Y. Lee and H.-J. Ahn, *J. Mater. Chem. A* **2017**, 5, 19714.

[18] Y.-W. Lee, B.-S. Kim, J. Hong, H. Choi, H.-S. Jang, B. Hou, S. Pak, J. Lee, S.-H. Lee, S. M. Morrisa, D. Whang, J.-P. Hong, H.S. Shin, S.N. Cha, J. I. Sohn, J.M. Kim, *Nano Energy* **2017**, 37, 15.

[19] G.-H. An, H.-J. Ahn, *Appl. Surf. Sci.* **2019**, 473, 77.

[20] G.-H. An, D.-Y. Lee, H.-J. Ahn, *J. Ind. Eng. Chem.* **2018**, 65, 423.

[21] G.-H. An, H.-J. Ahn, *Carbon* **2013**, 65, 87.

[22] T. Scarazzato, Z. Panossian, J.A.S. Tenório, V. Pérez-Herranz, and D.C.R. Espinosa, *J. Cleaner Prod.* **2017**, 168, 1590.

[23] Z Chen, S. Ye, A. R. Wilson, Y.-C. Ha and B. J. Wiley, *Energy Environ. Sci.* **2014**, 7, 1461.

[24] Y. Chen, T. Zhou, Y. Liu and Z. Guo, *J. Mater. Chem.* A **2017**,5, 23476.

[25] Z. Chen, P. Kang, M.-T. Zhang, B.R. Stoner and T.J. Meyer, *Energy Environ. Sci.* **2013**,6, 813.

[26] T. Shimizu, Y. Tada, N. Kaneko, S. Tanaka, S. Shingubara, *Surf. Coat. Technol.* **2016**, 294, 83.

[27] N. C. Maile, R.T. Patil, S.K. Shinde, D.-Y. Kim, A.V. Fulari, D.S. Lee, V.J. Fulari, *J. Mater. Sci.: Mater. Electron.* **2019**, 30, 5555.

[28] M.A. El-Jemni a, H.S. Abdel-Samad, A.S. Essa, H.H. Hassan, *Electrochim. Acta* **2019**, 313, 403.

[29] N. Alias, A.A. Mohamad, *J. King Saud Univ., Eng. Sci.* **2015**, 27, 43.

[30] J. Yang, Y. Wang, J. Kong, H. Jia, Z. Wang, *Opt. Mater.* **2015**, 46, 179.

[31] K. Zhao, C. Wang, Y. Yu, M. Yan, Q. Wei, P. He, Y. Dong, Z. Zhang, X. Wang, L. Mai, *Adv. Mater. Interfaces* **2018**, 23, 1800848.

[32] C. Lu, Y. Jin, X. Tao, B. Yang, G. Ye, *CrystEngComm* **2018**,20, 122.

[33] H.-S. Chou, K.-D. Yang, S.-H. Xiao, R.A. Patil, C.-C. Lai, W.-C.V. Yeh, C.-H. Ho, Y.Liou, Y.-R. Ma, *Nanoscale* **2019**, 11, 13385.

[34] R.S. Devan, J.-H. Lin, Y.-J. Huang, C.-C. Yang, S.Y. Wu, Y.Liou, Y.-R. Ma, *Nanoscale* **2011**, 3, 4339.

[35] P. Li, Z. Fang, Y. Zhang, C. Mo, X. Hu, J. Jian, S. Wang, D. Yu, *J. Mater. Chem. A* **2019**, 7, 17292.

[36] G.-H. An, D.-Y. Lee and H.-J. Ahn, *ACS Appl. Mater. Interfaces* **2017**, 9, 12478.

[37] X. Wang, Q. Li, L. Zhang, Z. Hu, L. Yu, T. Jiang, C. Lu, C. Yan, J. Sun and Z. Liu, *Adv. Mater.* **2018**, 30, 1800963.

[38] L. Que, Z. Wang, F.Y. and D. Gu, *J. Mater. Chem. A* **2016**, 4, 8716.

[39] V. Aravindan, N. Shubha, W.C. Ling and S. Madhavi, *J. Mater. Chem. A* **2013**, 1, 6145.

[40] H. Kim, M.-Y. Cho, M.-H. Kim, K.-Y. Park, H. Gwon, Y. Lee, K.C. Roh and K. Kang, *Adv. Energy Mater.* **2013**, 3, 1500.

[41] M. Yang, Y. Zhong, J. Ren, X. Zhou, J. Wei and Z. Zhou, Adv. *Energy Mater.* **2015**, 5, 1500550.

[42] D.P. Dubal, K. Jayaramulu, R. Zboril, R.A. Fischer and P. Gomez-Romero, *J. Mater. Chem. A* **2018**, 6, 6096.

[43] P. Pazhamalai, K. Krishnamoorthy, V.K. Mariappan, S.-J. Kim, *J. Ind. Eng. Chem.* **2018**, 64, 134.

[44] C. Liu, C. Zhang, H. Song, C. Zhang, Y. Liu, X. Nan, G. Cao, *Nano Energy* **2016**, 22, 290.

[45] J. Niu, R. Shao, M. Liu, J. Liang, Z. Zhang, M. Dou, Y. Huang, F. Wang, *Energy Storage Materials* **2018**, 12, 145.

[46] Y. Zhao, Y. Cui, J. Shi, W. Liu, Z. Shi, S. Chen, X. Wang and H.i Wang, *J. Mater. Chem. A* **2017**, 5, 15243.

[47] F. Wang, Z. Liu, X. Wang, X. Yuan, X. Wu, Y. Zhu, L. Fu and Y. WuD, *J. Mater. Chem. A* **2016**, 4, 5115.

[48] J.H. Won, H.M. Jeong and J.K. Kang, *Adv. Energy Mater.* **2017**, 7, 1601355.

[49] T. Chen, L. Qiu, Z. Yang, Z. Cai, J. Ren, H. Li, H. Lin, X. Sun and H. Peng, *Angew. Chem. Int. Ed.* **2012**, 51, 11977.

[50] V.T. Le, H. Kim, A. Ghosh, J. Kim, J. Chang, Q.A. Vu, D.T. Pham, J.-H. Lee, S.-W. Kim and Y. H. Lee, *ACS nano* **2013**, 7, 5940.

[51] Y. Huang, H. Hu, Y. Huang, M. Zhu, W. Meng, C. Liu, Z. Pei, C. Hao, Z. Wang and C. Zhi, *ACS nano* **2015**, 9, 4766.

[52] L. Kou, T. Huang, B. Zheng, Y. Han, X. Zhao, K. Gopalsamy, H. Sun and C. Gao, *Nat. Commun.* **2014**, 5, 3754.

[53] Q. Meng, H. Wu, Y. Meng, K. Xie, Z. Wei and Z. Guo, *Adv. Mater.* **2014**, 26, 4100.

[54] K. Guo, Y. Ma, H. Li and T. Zhai, *Small* **2016**, 12, 1024.

[55] J. Ren, W. Bai, G. Guan, Y. Zhang and H. Peng, *Adv. Mater.* **2013**, 25, 5965.

[56] Y. Chang, G. Han, Y. Xiao, H. Zhou, M. Li, D. Fu and W.Zhou, *New Carbon Materials* **2017**, 32, 581.

[57] X. Pu, L. Li, M. Liu, C. Jiang, C. Du, Z. Zhao, W. Hu and Z.L. Wang, *Adv. Mater.* **2016**, 28, 98.

[58] Y. Meng, Y. Zhao, C. Hu, H. Cheng, Y. Hu, Z. Zhang, G. Shi and L. Qu, *Adv. Mater.* **2013**, 25, 2326.

[59] S. Dai, H. Guo, M. Wang, J. Liu, G. Wang, C. Hu and Y Xi, *J. Mater. Chem. A* **2014**, 2, 19665.

[60] P. Xu, T. Gu, Z. Cao, B. Wei, J. Yu, F. Li, J.-H. Byun, W. Lu, Q. Li and T.-W. Chou, *Adv. Energy Mater.* **2014**, 4, 1300759.

[61] J. Bae, M.K. Song, Y.J. Park, J.M. Kim, M. Liu and Z.L.Wang, *Angew. Chem. Int. Ed.* **2011**, 50, 1683.

Figure caption

Figure 1 (a) Schematic illustration and Ragone plots of flat-type ZICs (b) Schematic illustration of two-dimensionally and hierarchically nanostructured Zn (2D-Zn) metal electrode.

Figure 2 Current curve of (a) 2D-Zn/1.0, (b) 2D-Zn/1.8, and (c) 2D-Zn/1.8/1.0 during by a voltage-tailored electroplating method. SEM images of (d) 2D-Zn/1.0, (e) 2D-Zn/1.8, and (f) 2D-Zn/1.8/1.0. (g) XRD patterns of 2D-Zn. XPS spectra of (h) Zn 2p and (i) Ni 2p for 2D-Zn.

Figure 3 (a) Nyquist plots in the frequency before charge−discharge tests. (b) Cyclic voltammetry (CV) curves at scan rate of 10 mV s^{-1} in the potential range 0.2 to 1.8 V. (c) Calculated specific capacitance at current densities in the range from 0.5 to 20.0 A g^{-1} in the potential range 0.2 to 1.8 V. (d) Ragone plots related to energy and power densities ranging from 500 to 20,000 W kg^{-1}. (e) Cycling stability at the current density of 10.0 A g^{-1} over 10,000 cycles.

Figure 4 (a) Schematic illustration of flat-type ZICs, including the 2D-Zn@CF as anode, AC@CF as cathode, cellulose paper as separator, $ZnSO_4$-PVA gel as electrolyte, and thermally shrinkable tube as cell case. (b) SEM images of 2D Zn@CF consisting of 2D Zn nanostructures grown on the CF by an electroplating. (c) XRD patterns of 2D-Zn@CF. (d) XPS spectra of Zn 2p for 2D-Zn@CF.

Figure 5 (a) Ragone plots related to energy and power densities ranging from 50 to 3,000 μW cm^{-2}. (b) Cycling stability at the current density of 1.0 mA cm^{-2} over 10,000 cycles. (c) Capacitance retention on the straight, folded, and knotted states. (d) Capacitance retention obtained in water for 15 h. (e) Light emitting diode powered by serially and parallelly connected fiber-type ZICs at knotted state in water.

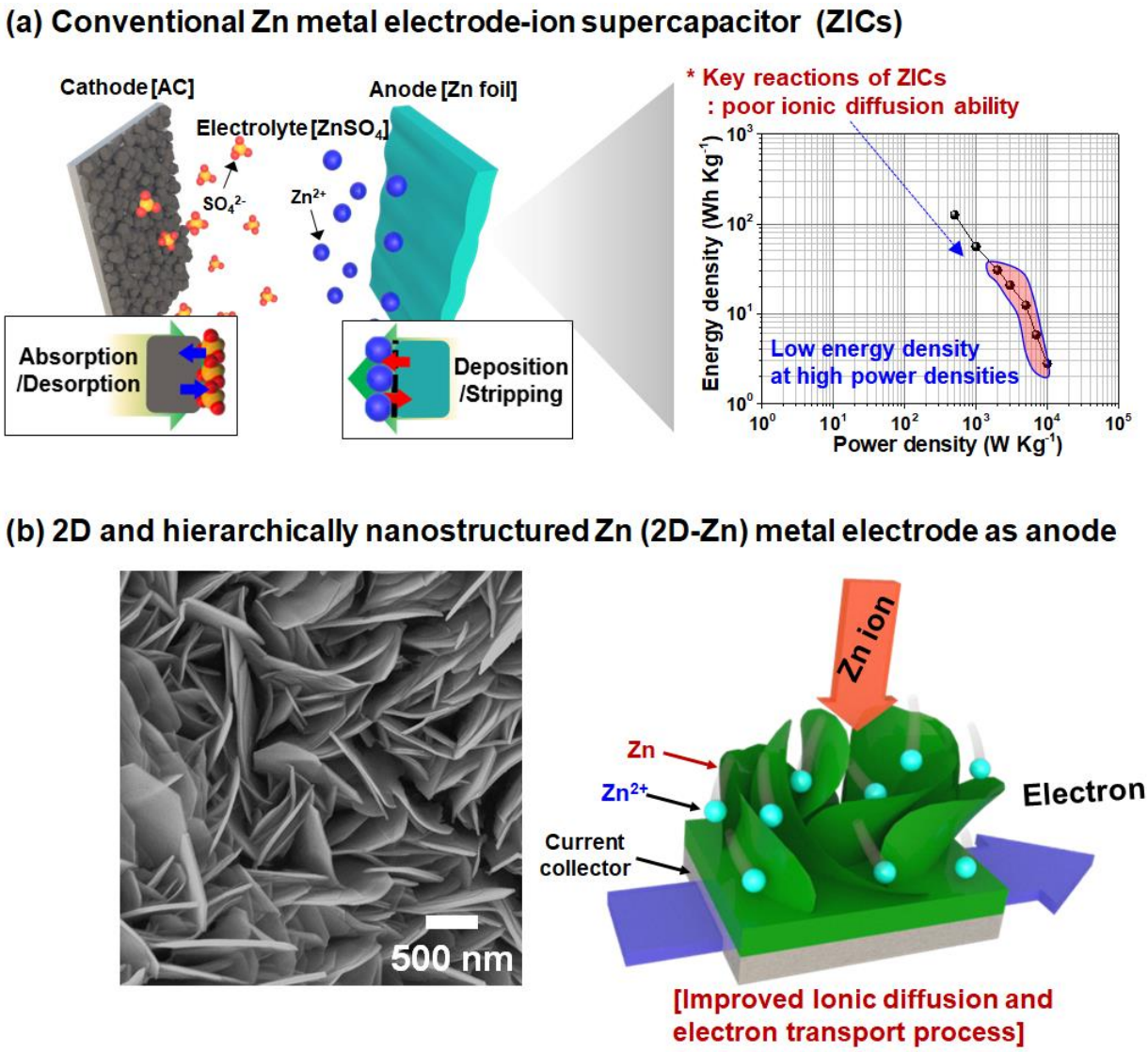

Figure 1 An *et al*.

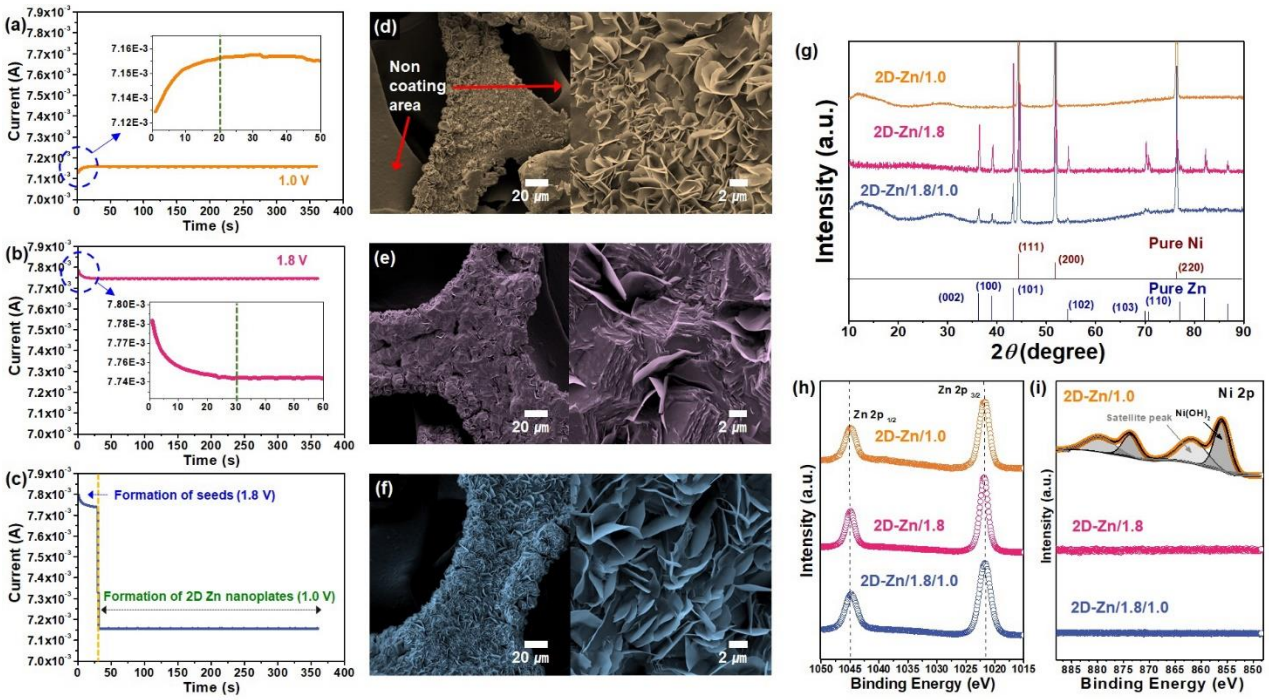

Figure 2 An *et al*.

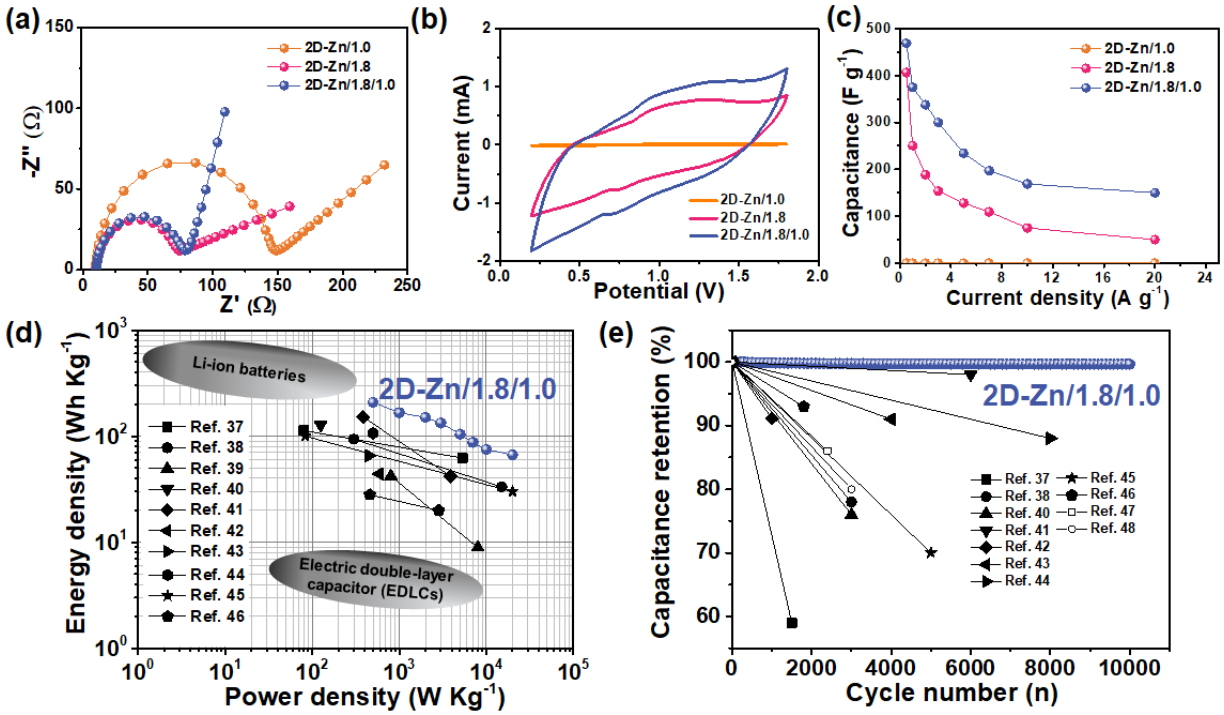

Figure 3 An *et al*.

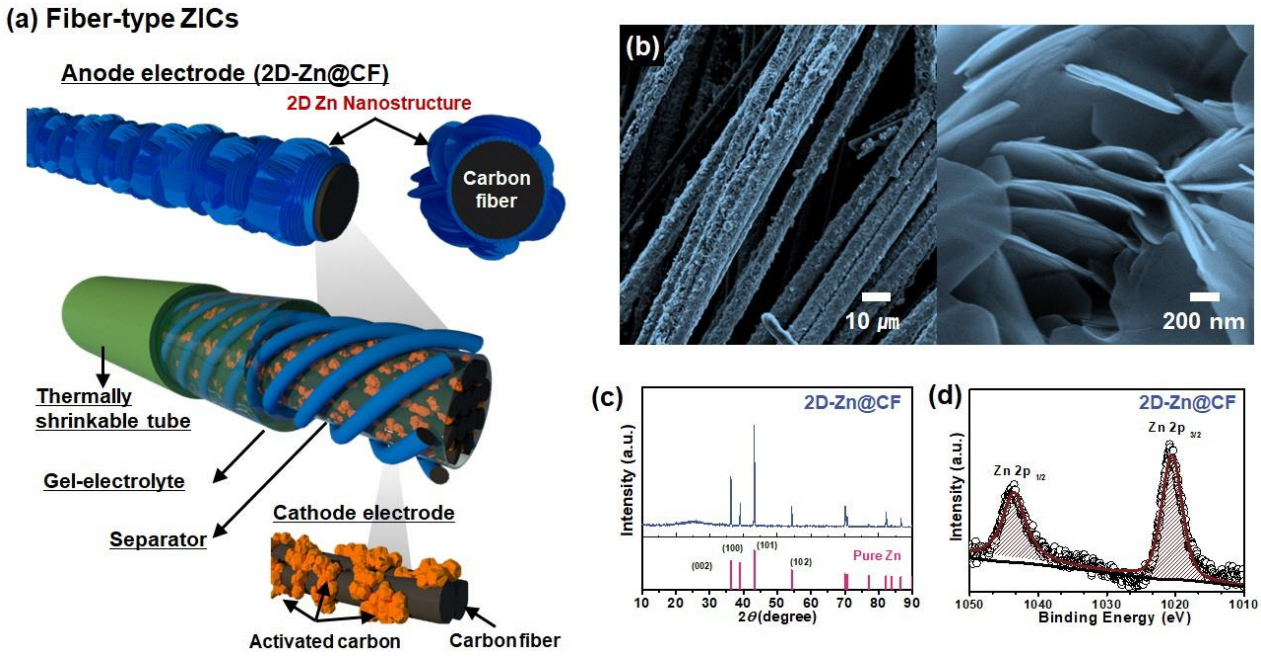

Figure 4 An *et al*.

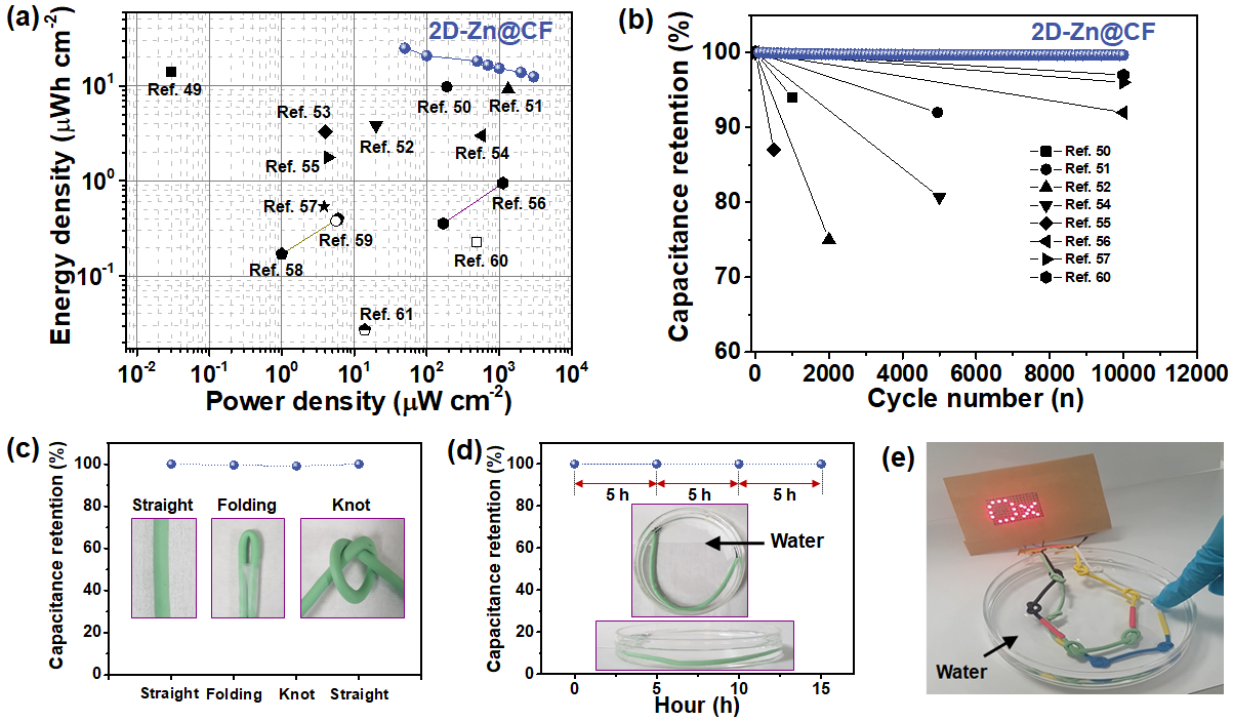

Figure 5 An *et al*.